Journal of Molecular Structure 1225 (2021) 129139

Contents lists available at ScienceDirect

Journal of Molecular Structure

journal homepage: www.elsevier.com/locate/molstr

A new Pd(II)-Hydrazide-Triphenylphosphine complex: Synthesis, crystal structure, spectroscopic characterization and theoretical calculations

Gökhan Dikmen[a,*], Hakan Ünver[b]

[a] Central Research Laboratory Application and Research Center (ARUM), Eskisehir Osmangazi University, Eskisehir, 26040, Turkey
[b] Department of Chemistry, Faculty of Science, Eskisehir Technical University, Eskisehir, 26040, Turkey

ARTICLE INFO

Article history:
Received 17 May 2020
Revised 19 August 2020
Accepted 21 August 2020
Available online 25 August 2020

Keywords:
Palladium
X-ray
Spectroscopic characterization
DFT

ABSTRACT

A new palladium(II) complex, $[Pd(PPh_3)(4\text{-}NO_2\text{-}BZH)Cl_2]$, bearing 4-Nitrobenzhydrazide and triphenylphosphine ligands has been synthesized and mainly characterized with single crystal X-ray diffraction analysis, FT-IR, Raman and NMR spectroscopic methods. Theoretical calculations were performed to explain chemical structure and vibrational properties. The geometric optimization, vibrational wavenumbers and chemical shift values of the title compound were investigated using the DFT/ B3LYP method, 6-311G++(d,p) and LanL2DZ level of theory. An agreement between the experimental and the theoretical results was observed. The high chemical reactivity of the title compound was theoretically examined by calculating the chemical potential, electrophilicity index, chemical hardness and global electrophilicity index.

1. Introduction

Palladium complexes have unique physical and chemical properties and because of these features, they have been studied in many different fields such as industry, medicine, pharmacy and continue to be studied [1–4]. In recent years, especially anticarcinogenic properties of palladium complexes are studied. Because these complexes have been observed that many different Pd(II) complexes have a high degree of cytotoxicity against various cancer cells. For instance, programmed cell death was observed in MCF-7 cells by the new synthesized palladium complexes [5]. Moreover, Pd complex has also excellent anticancer activity for lung cancer AGZY-83a [6].

Hydrazides have been widely used in the literature because of their biological activities. When hydrazides are used with metal complexes, metal complexes increase their biological activities [7,8]. Due to the functional groups C=O, NH and NH_2 in the structure of hydrazides, they provide various potentially active donor sites [9,10]. Hydrazides and their derivatives along with metallic complexes have an important role in the improvement of their biological activities. Many metal complexes of hydrazides show biological properties [11–13]. Metal complexes of hydrazides indicate especially antimicrobial activity. In the literature, hydrazide ligands and their respective Pd(II) complexes were synthesized and obtained complexes used to determine α-glucosidase and carbonic anhydrase II enzyme inhibition activities [14]. Moreover, Pd(II) and Pt(II) complexes of hydrazide derivative of ibuprofen were inactive over Staphylococcus aureus, Escherichia coli and Pseudomonas aeruginosa bacterial strains whereas $[PdCl_2(HIB)_2]$ complex was active over ovarian cancer cell line [15]. However, in some studies, it has been observed that molecules formed by hydrazides and Pt complexes have highly effective anticarcinogenic properties on some cancer cells [16–18]. In the literature, a few examples of 4 nitrobenzoic hydrazide complexes with Pt and Pd atoms have been reported and obtained complexes showed cytotoxicity against K562 tumoral cell line and it is concluded that these complexes are significantly more cytotoxic than cisplatin [19]. On the other hand, 4-hydroxybenzhydrazide (4-OH-BZH) is hydrazine derivative molecule and it is well known for different applications such as biological, analytical and agricultural. In the literature, the most famous hydrazide is the isonicotinic acid hydrazide. Because this molecule has been used as anti-tuberculosis drug. Nitro group containing hydrazides show anticancer activity [18]. Moreover, there are various studies about Cu(II) and Ni(II) complexes with 4hbah molecule, as well [20,21].

Density Functional Theory (DFT) calculations have been used in structural characterization of molecular systems, interactions of intra and inter molecules. Moreover, DFT is effective method for determination of physical and chemical properties of molecules.

* Corresponding author.
E-mail address: gdikmen@ogu.edu.tr (G. Dikmen).

https://doi.org/10.1016/j.molstruc.2020.129139
0022-2860/

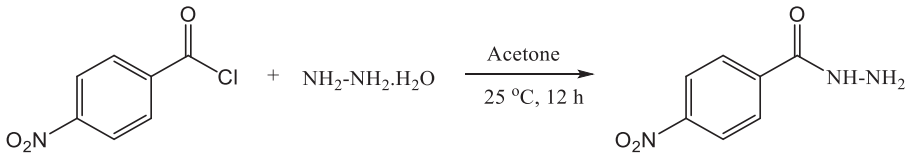

Fig. 1. Synthesis of 4-nitrobenzhydrazide (4-NO_2-BZH) ligand.

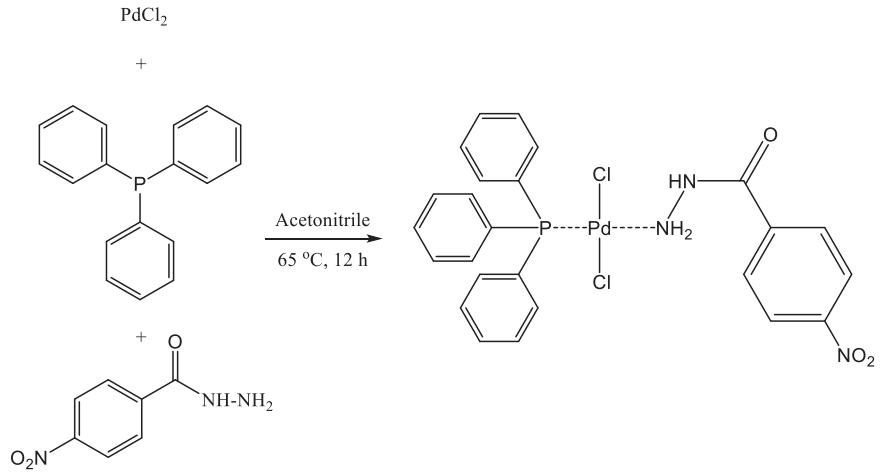

Fig. 2. Synthesis of [$Pd(PPh_3)$(4-NO_2-BZH)Cl_2] complex.

In many studies, it was observed that the results obtained theoretically and experimentally were compatible with each other by combining spectroscopic characterization methods and DFT calculations [22–28].

Various new complexes containing Pd atom are still being researched in the literature due to their very high biological activities. Therefore, A new palladium(II) complex, [$Pd(PPh_3)$(4-NO_2-BZH)Cl_2], bearing 4-Nitrobenzhydrazide and triphenylphosphine ligands has been synthesized and characterized herein. In this study, we present the synthesis, crystallographic structure and spectroscopic characterization of [$Pd(PPh_3)$(4-NO_2-BZH)Cl_2]. Title compound was characterized using single crystal X-ray diffraction (XRD), FT-IR, Raman and NMR spectroscopic methods. DFT is used to determine structure analysis.

2. Experimental

2.1. Reagents and apparatus

Palladium(II) chloride (99%), triphenylphosphine (99%), 4-nitrobenzoyl chloride (99%), hydrazine monohydrate (98%), phenylacetic acid (99%) and sodium hydroxide (>97%) were purchased from Sigma Aldrich.

2.2. Complex synthesis

Ligand and its palladium complex synthesis procedure is given in Figs. 1 and 2.

2.2.1. Synthesis of 4-nitrobenzhydrazide (4-NO_2-BZH)

Ligand synthesis was conducted by following the published data with slight modifications [29]. The reaction between equimolar ratio of 4-nitrobenzoyl chloride (1 eq, 500 mg, 2.7 mmol) and hydrazine monohydrate (1 eq, 135 mg 2.7 mmol) in anhydrous acetone at 25 °C for 12 h resulted in the desired product in high yields. (316 mg; Yield: 65%; m.p.: 216 °C), Anal. Calc.: $C_7H_7N_3O_3$: C, 46.41%; H, 3.90%; N, 23.20%. Found: C, 46.59%; H, 3.79%; N, 23.45%. ^{1}H-NMR spectra of 4-NO_2-BZH molecule was given in Fig. S1.

2.2.2. Synthesis of the palladium (II) complex, [$Pd(PPh_3)$(4-NO_2-BZH)Cl_2]

To the anhydrous 10 mL acetonitrile solution of palladium(II) chloride ($PdCl_2$) (1 eq, 50 mg, 0.28 mmol) which was stirred for 30 min at 65 ºC, 4-nitrobenzhydrazide (1 eq, 51 mg, 0.28 mmol) solution in 10 mL acetonitrile was added drop by drop over 5 min. Resulting mixture was left to stir for 1 h at the same temperature. After this, triphenylphosphine (PPh_3) (1 eq, 74 mg, 0.28 mmol) solution in the same solvent was added over 5 min and the resulting clear orange mixture was left for stirred overnight under reflux temperature. After the completion of the reaction, the mixture was left for slow evaporation of the solvent and X-ray suitable dark orange cubic crystals were obtained. (91 mg; Yield: 52%); Anal. Calc.: $C_{25}H_{22}Cl_2N_3O_3PPd$: C, 48.37%; H, 3.57%; N, 6.77%. Found: C, 48.62%; H, 3.45%; N 6.58%. ^{1}H NMR spectra of PPh_3 molecule was given in Fig. S2.

2.3. X-ray Data Collection and Structure Refinement

Single crystal X-ray diffraction data of Pd(II) complex was collected with Bruker AXS APEX-II CCD diffractometer equipped with a rotating anode at 296.15 K (Mo-Kα radiation at λ = 0.71073 Å). Data integration was done with the Bruker SMART program package [30]. Using Olex2 software [31], structure solution was done with ShelXS [32] using DirectMethods and refinement was done with ShelXL [33] refinement package using Least Squares minimization. Ellipsoid structure of complex was drawn at MERCURY program [34].

2.4. Characterization details

FT-IR spectrum was collected with Perkin Elmer Spectrum Two using KBr pellets, range from 4000 to 400 cm^{-1} having 4 cm^{-1}

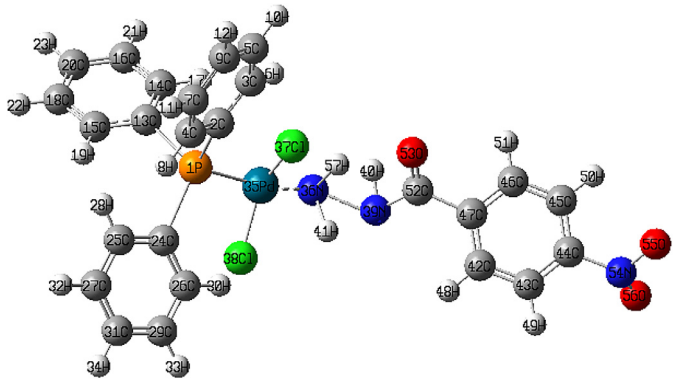

Fig. 3. Chemical structure of Pd(II)-Hydrazide-Triphenylphosphine Compound.

resolution. Raman spectrum was obtained by a Renishaw Invia Raman microscope spectrometer with 532 nm excitation between 4000 and 400 cm^{-1} at a resolution of 4 cm^{-1}. Thermal analysis of the complex was conducted using Perkin Elmer STA 8000. TG and DTG curves were obtained in a static air atmosphere at a heating rate of 10 $K.min^{-1}$ in the temperature range from 25 °C to 600 °C using platinum crucible. NMR spectra were collected with JEOL ECZ 500R. d_6-DMSO and tetramethylsilane (TMS) were used as solvent and internal standard, respectively.

2.5. Computational details

Geometric optimization, vibrational frequencies and geometric parameters of title compound were calculating using Gaussian 09 program package [35]. The valence triple-zeta basis set augmented with diffuse and polarization functions in both the hydrogen and weighty atoms 6–311++G(d,p) has been used for geometry optimization and vibrational frequency calculations. The LanL2DZ basis set augmented with polarization and diffuse functions was used for the Pd atom, with the core orbitals replaced by Effective Core Potentials (ECP) [36]. Vibrational frequencies were scaled with Scaled Quantum Mechnanical (SQM) program [37–40] to generate the corrected frequencies. The fundamental vibrational modes were assigned and the total energy distribution (TED) calculations were performed by the SQM. Chemical structure of title compound is given in Fig. 3.

3. Results and discussions

3.1. Single crystal X-ray analysis

The reaction of palladium(II) chloride ($PdCl_2$), 4-nitrobenzhydrazide (4-NO_2-BZH) and triphenylphosphine (PPh_3) resulted in air and moisture stable palladium(II) complex ([$Pd(PPh_3)$(4-NO_2-BZH)Cl_2]) in high yields. Complex absolute structure was mainly characterized with X-ray diffraction besides other spectroscopic techniques (NMR, FT-IR. Elemental analysis). Crystal data, refinement parameters, selected bond distances and bond angles are presented in Tables 1 and 2. Complex ChemDraw and ORTEP structures are given in Fig. 4.

ORTEP structures of Pd(II) complex is depicted in Fig. 4. The complex crystallising in the triclinic, P-1 space group contains two independent molecules with slightly distorted square planar geometry relative to the metal center. Central atom surrounded with phosphorus (P1) and nitrogen (N1) atoms of two separate ligands in *trans*- positions and two chlorine ions (Cl1 and Cl2) as counter anions. Measured bond distances between Pd(1)-P(1), Pd(1)-Cl(1), Pd(1)-Cl(2), Pd(1)-N(1) atoms are 2.232, 2.280, 2.281 and 2.138 Å, respectively. The bond length of palladium-phosphine

Table 1
Crystal data and structure refinement for the [$Pd(PPh_3)$(4-NO_2-BZH)Cl_2] complex.

Empirical formula	$C_{25}H_{22}Cl_2N_3O_3PPd$
Formula weight	620.73
Temperature	296 K
Wavelength	0.71073 Å
Crystal system, space group	triclinic, P-1
Unit cell dimensions	a = 10.1056(4) Å alpha = 86.005(2) ° b = 12.1848(5) Å beta = 78.535(2) ° c = 22.6523(8) Å gamma = 67.901(2) °
Volume	2532.76(17) A^3
Z, Calculated density	2, 1.628 Mg/m^3
Absorption coefficient	1.040 mm^{-1}
F(000)	1248.0
Crystal size	0.08 x 0.06 x 0.04 mm
Theta range for data collection	1.834 to 56.79 deg.
Limiting indices	-13<=h<=13, -16<=k<=16, -29<=l<=30
Reflections collected / unique	51607/12659 [R(int) = 0.0287]
Completeness to theta	28.395 99.4%
Absorption correction	Integration
Refinement method	Full-matrix least-squares on F^2
Data / restraints / parameters	12659 / 0 / 631
Goodness-of-fit on F^2	1.027
Final R indices [I>2sigma(I)]	R1 = 0.0332, wR2 = 0.0803
R indices (all data)	R1 = 0.0474, wR2 = 0.0887
Largest diff. peak and hole	1.01 and -0.60 $e.A^{-3}$

Table 2
Selected intramolecular bond distances (Å), bond angles and intermolecular hydrogen bonds of [$Pd(PPh_3)$(4-NO_2-BZH)Cl_2] complex

Parameters	Experimental	Calculated
Bond Lengths (A)		
Pd(1)-P(1)	2.232(6)	2.251
Pd(1)-Cl(1)	2.280(7)	2.306
Pd(1)-Cl(2)	2.281(7)	2.308
Pd(1)-N(1)	2.138(4)	2.153
P(1)-C(26)	1.812(2)	1.844
P(1)-C(32)	1.811(2)	1.844
P(1)-C(38)	1.814(2)	1.845
N(1)-N(2)	1.401(3)	1.416
N(2)-C(44)	1.326(3)	1.339
C(44)-O(1)	1.218(3)	1.240
C(48)-N(3)	1.467(3)	1.471
N(3)-O(3)	1.213(3)	1.226
N(3)-O(2)	1.208(4)	1.294
Bond Angles (°)		
P(1)-Pd(1)-Cl(1)	94.85(2)	86.55
Cl(1)-Pd(1)-N(1)	90.52(6)	97.98
N(1)-Pd(1)-Cl(2)	88.28(6)	97.96
Cl(2)-Pd(1)-P(1)	86.28(2)	86.55
C(26)-P(1)-Pd(1)	113.94(8)	115.28
C(32)-P(1)-Pd(1)	106.95(8)	112.68
C(38)-P(1)-Pd(1)	118.77(8)	112.68
Pd(1)-N(1)-N(2)	116.01(14)	115.96
N(1)-N(2)-C(44)	121.90(2)	120.63
N(2)-C(44)-O(1)	122.22(2)	125.36
O(1)-C(44)-C(45)	122.65(2)	125.36
C(48)-N(3)-O(2)	118.53(3)	115.83
C(48)-N(3)-O(3)	117.80(3)	115.83
O(3)-N(3)-O(2)	123.70(3)	124.08
Cl(1)-Pd-Cl(2)	177.54(3)	150.38
P(1)-Pd-N(1)	174.27(6)	
Torsion Angles (°)		
Pd-N1-N2-C4	-178.2(2)	0.00
P-Pd-N1-N2	-170.0(5)	-179.99
O2-N3-C48-C47	6.20	0.00
C26-P-Pd-C12	59.52(10)	0.00
Hydrogen bonding interactions (Å)		
C(44)-O(1)--H1A 3.056		
N(3)-O(3)--H1B 3.001		
N(6)-O(6)--H2 3.070		

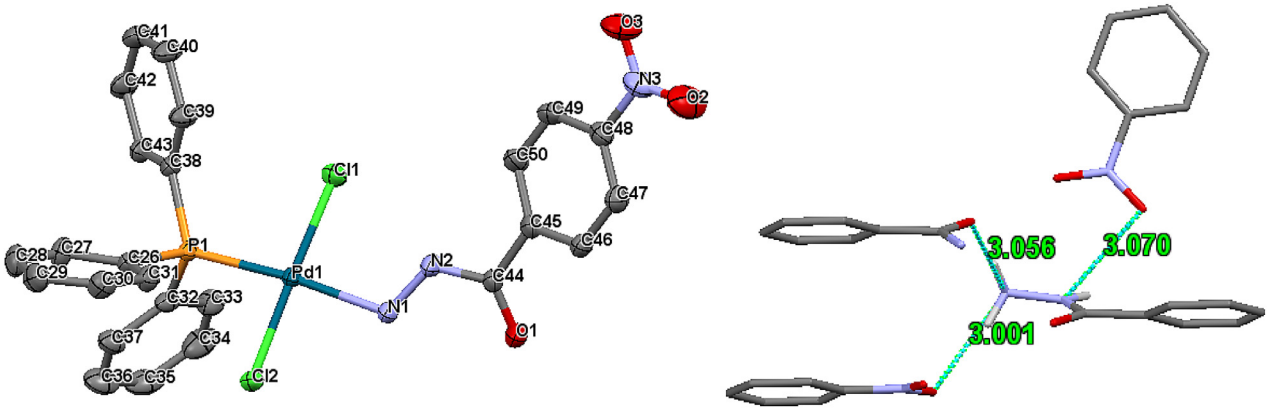

Fig. 4. [$Pd(PPh_3)(4\text{-}NO_2\text{-}BZH)Cl_2$] complex a) molecular structure with 30% thermal ellipsoid probability level and b) intermolecular hydrogen bonding interactions.

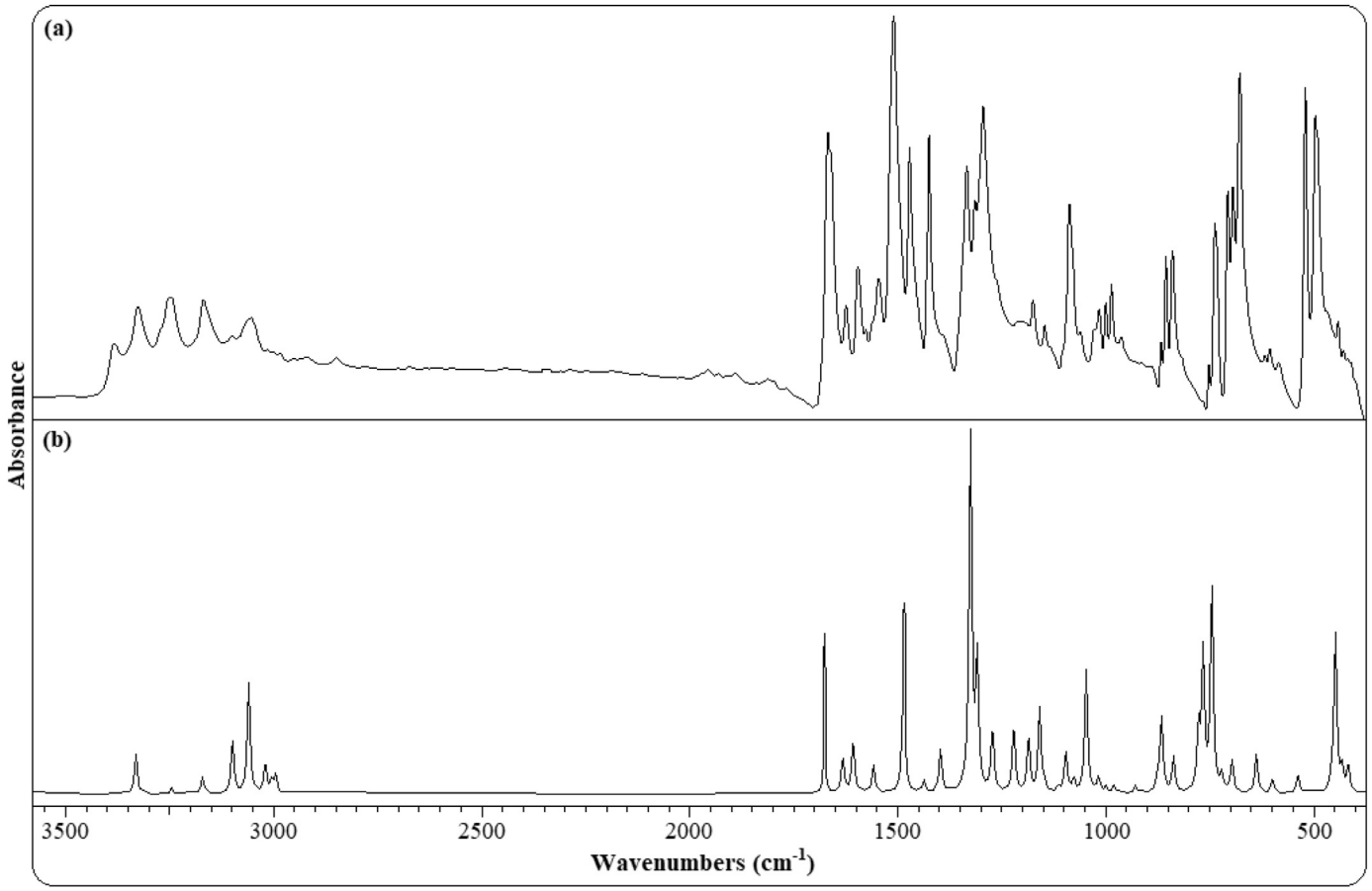

Fig. 5. Experimental (a) and theoretical (b) IR spectra of title compound.

(Pd(1)-P(1) = 2.232 Å) is longer than palladium-hydrazide (Pd(1)-N(1) 2.138 Å) and these values are found to be similar with literature reports [41]. In addition, some intermolecular hydrogen bonding interactions were observed between nitro (-NO_2) and carbonyl (-C=O) oxygens and amine parts of hydrazide (NH_2 and NH) ligand which were responsible for the stabilization of crystal structure (Fig. 4). The distances of measured hydrogen bonds are listed in Table 2. The coordination angles between metal center and donor atoms (P(1)-Pd(1)-Cl(1), Cl(1)-Pd(1)-N(1), N(1)-Pd(1)-Cl(2) and Cl(2)-Pd(1)-P(1)) vary between 86.28 - 94.85º. The deviation of angles to bigger than 90º at P(1)-Pd(1)-Cl(1) = 94.85º and Cl(1)-Pd(1)-N(1) = 90.52º is due to the steric effect of both phosphine and tail part of hydrazide ligand.

3.2. Vibrational studies

3.2.1. N-H vibrations

Theoretical and experimental IR and Raman spectra of title molecule are given in Figs. 5 and 6, respectively. NH stretching modes are seen in the range from 3300 cm^{-1} to 3600 cm^{-1} in the literature [42]. In this study, NH stretching modes were observed at 3385 and 3328 cm^{-1} in the IR spectrum, 3379 and 3329 cm^{-1} in the Raman spectrum and the NH stretching modes were calculated to have frequencies 3387 and 3331 cm^{-1}, respectively. Asymmetric NH vibration peaks are observed have higher intensity than the symmetric NH vibration peak in the IR spectrum whereas the symmetric NH vibration peaks are observed as more intensity in

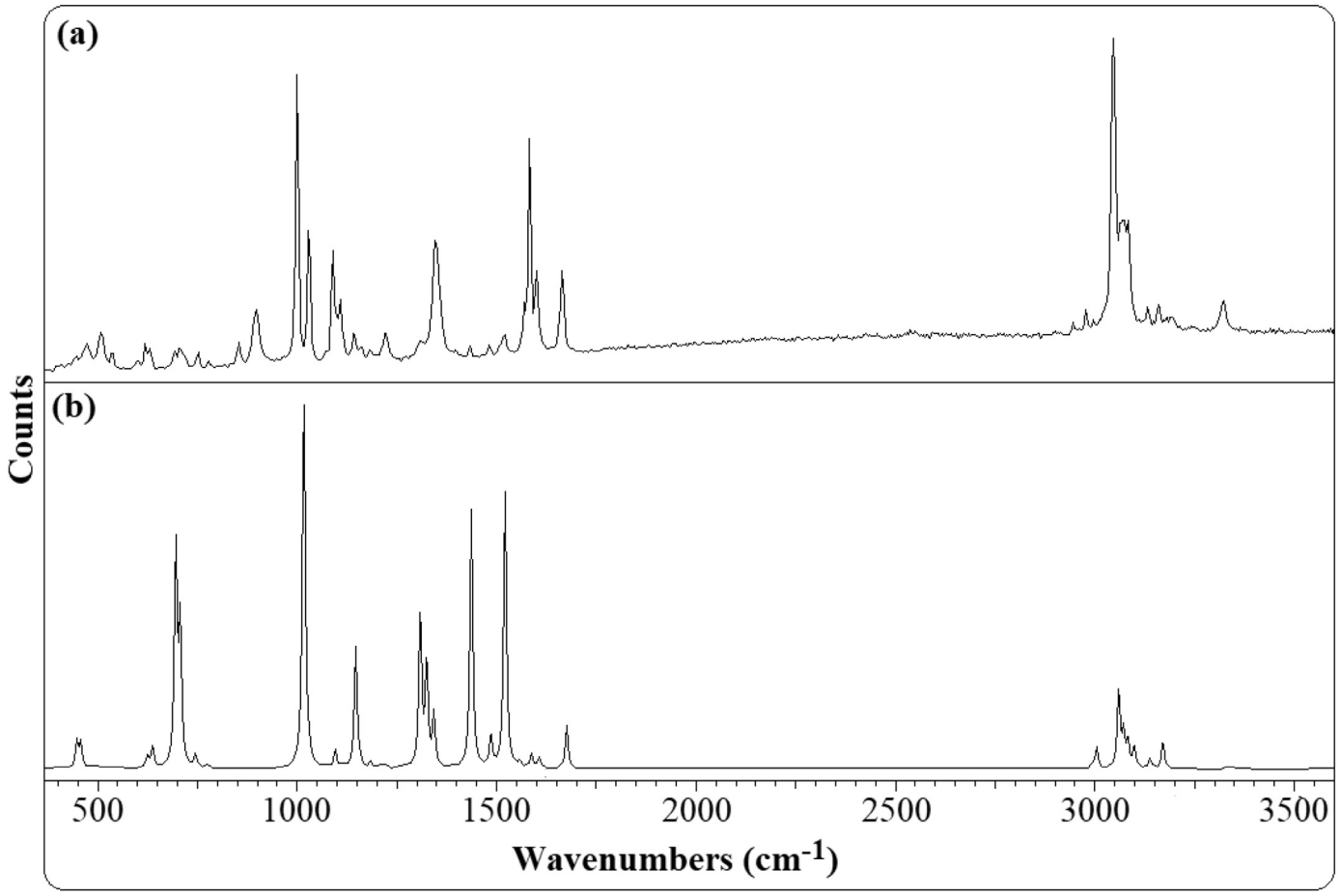

Fig. 6. Experimental (a) and theoretical (b) Raman spectra of title compound.

the Raman spectrum, because electronic polarizability of NH symmetric vibrational form changes more than NH asymmetric vibrational form and so differences in band are observed [43]. Similar observations were also reported in previous works [44,45]. Moreover, NH-in plane bending mode was observed at 1221 cm^{-1} in the IR spectrum, at 1224 cm^{-1} in the Raman spectrum and this mode was calculated as 1219 cm^{-1} in this study. The NH out of plane-bending mode was calculated to be 638 cm^{-1}. The band was observed experimentally at 629 cm^{-1} in the IR spectrum, 630 cm^{-1} in the Raman spectrum. NH torsion mode was seen at 532 cm^{-1} in the IR spectrum and at 533 cm^{-1} in the Raman spectrum and calculated as 538 cm^{-1}.

3.2.2. C-H vibrations

In general, CH stretching vibrations for aromatic compounds are observed in the range from 3100 to 3000 cm^{-1} [46–50]. In this study, CH stretching modes of title compound were seen between 3247 and 2986 cm^{-1} in the IR spectrum and observed between 3170 and 2954 cm^{-1} in the Raman spectrum. CH stretching vibrations were computed between 3245 and 2995 cm^{-1}. The vibrations observed at 1185 and 974 cm^{-1} in the IR spectrum and observed at 1181 cm^{-1} in the Raman spectrum are where intense bands arising from out-of-plane C–H bending vibrational modes. Moreover, CH in plane vibrational mode of title compound was observed at 1272 cm^{-1} in the IR spectrum and this band was not observed in the Raman spectrum. CCH bending vibrations were seen at 1480 and 1433 cm^{-1} in the IR spectrum and observed at 1483 and 1433 cm^{-1} in the Raman spectrum. HCH bonding vibration of title compound was observed at 1518 cm^{-1} in the IR spectrum, 1522 cm^{-1} in the Raman spectrum. Theoretical wavenumbers and experimentally obtained these wavenumbers are given in Table 3. All results for CH stretching are in agreement with the literature [51].

3.2.3. NO_2 vibrations

The asymmetric NO stretching modes of nitro group are observed in the range from 1570 to 1485 cm^{-1} and symmetric stretching modes are observed between 1370 and 1320 cm^{-1} [52]. In this study, the asymmetric stretching of nitro group was seen at 1585 and 1586 cm^{-1} in the IR and Raman spectra, respectively. The symmetric stretching mode of nitro group was observed at 1343 cm^{-1} in the IR spectrum and observed at 1348 cm^{-1} in the Raman spectrum.

The deformation mode of nitro group was seen at 851 cm^{-1} in the IR spectrum, at 854 cm^{-1} in the Raman spectrum. The NO wagging mode was observed at 749 cm^{-1} in the IR spectrum and observed at 753 cm^{-1} in the Raman spectrum. Theoretical responses of these vibration motives are given in Table 3.

3.2.4. NN vibration

NN stretching bands were observed in the previous studies between 1350 and 1535 cm^{-1} [53,54]. In this study, NN stretching band was observed at 1304 cm^{-1} in the IR spectrum and at 1306 cm^{-1} in the Raman spectrum. This band was calculated as 1309 cm^{-1}. Intensity of this band is higher in the IR spectrum than Raman spectrum. Moreover, CNN in plane bending vibration of title compound was observed at 422 cm^{-1} in the IR spectrum, although this bending vibration was not seen in the Raman spectrum.

Table 3
Comparison of the experimental and calculated vibrational wavenumbers of title compound

	Assignments	Experimental		6-311++G(d,p)/LANL2DZ			
Modes	TED(≥10%)	IR	Raman	Unscaled	Scaled	I_{IR}	I_R
υ_1	υ(N-H)(98)	3385	3379	3569	3387	0.21	0.04
υ_2	υ(N-H)(98)	3328	3329	3511	3331	14.07	60.04
υ_3	υ(C-H)(100)	3247	-	3415	3245	2.07	-
υ_4	υ(C-H)(100)	3170	3170	3337	3170	6.29	138.69
υ_5	υ(C-H)(96)	-	3137	3298	3138	-	48.22
υ_6	υ(C-H)(95)	3103	3091	3261	3099	19.13	102.00
υ_7	υ(C-H)(93)	-	3082	3242	3083	-	128.65
υ_8	υ(C-H)(90)	-	3072	3230	3072	-	155.66
υ_9	υ(C-H)(85)	3056	3054	3221	3060	39.37	365.74
υ_{10}	υ(C-H)(80)	3016	-	3186	3020	11.04	-
υ_{11}	υ(C-H)(80)	3004	2987	3160	3005	4.21	97.01
υ_{12}	υ(C-H)(67)	2986	2954	3148	2995	6.75	20.84
υ_{13}	υ(C-O)(60)	1676	1668	1718	1676	13.12	141.80
υ_{14}	υ(C-N)(28) + β(C-H)(11)	1632	-	1675	1632	13.08	-
υ_{15}	β(C-H)(85) + υ (C-C)(14)	1604	1602	1648	1607	19.62	35.58
υ_{16}	υ(N-O)(53)	1585	1586	1626	1588	1.14	43.68
υ_{17}	β(C-H)(67) + υ (C-C)(16)	1554	1571	1594	1558	10.20	19.91
υ_{18}	υ(C-C)(74) + β (H-C-H)(22)	1518	1522	1555	1521		870.84
υ_{19}	υ(C-C)(57) + β (C-C-H)(65)	1480	1483	1529	1486	45.24	100.22
υ_{20}	β(H-C-H)(56)	1433	1433	1475	1437	4.39	788.78
υ_{21}	β(H-C-H)(36)+α(C-C-C)(14)	1397	-	1432	1397	15.68	-
υ_{22}	υ(N-O)(32)	1343	1348	1378	1343	1.06	157.22
υ_{23}	γ(C-H)(39)+ β (H-C-H)(10)	1323	-	1360	1325	127.31	325.14
υ_{24}	υ(N-N) (24)	1304	1306	1341	1309	46.27	479.22
υ_{25}	β(C-H)$_{\text{in plane}}$ (61)	1272	-	1311	1272	23.38	-
υ_{26}	β(N-H)(34)	1221	1224	1262	1221	24.72	12.99
υ_{27}	β(H-C-C)(52)	1185	1181	1218	1185	20.36	18.29
υ_{28}	β(C-C-H)(45)+ υ(C-C)(10)	1157	1161	1188	1159	29.83	14.09
υ_{29}	β(C-C-H)(30)	1142	1142	1175	1147	3.33	349.68
υ_{30}	υ(C-O)(10)	1114	1107	1146	1114	1.70	2.53
υ_{31}	υ(C-C)(28)	1097	1088	1128	1096	15.86	54.37
υ_{32}	β(H-C-H)(54)	1071	-	1101	1077	5.01	-
υ_{33}	β(C-C-H)(29)+τ(H-C-C-C)(10)	1039	-	1076	1047	43.56	-
υ_{34}	β(C-C-H)(42)	1026	1028	1058	1030	0.56	22.75
υ_{35}	β (H-C-C)(25)+ υ(C-C)(16)	1010	1000	1033	1017	5.68	999.97
υ_{36}	υ(C-C)(32)+ β(C-C-C)(15)	997	-	1026	999	2.46	-
υ_{37}	β(C-H)$_{\text{out of plane}}$(47)	974	-	1013	979	2.84	-
υ_{38}	υ(N-N)(27)	925	-	958	929	2.66	-
υ_{39}	τ(H-C-C-C)(32)	901	900	933	907	0.09	0.45
υ_{40}	β(ring)$_{\text{in plane}}$ (48)	878	-	898	875	4.73	-
υ_{41}	β(C-H)$_{\text{out of plane}}$(34)	866	-	881	866	27.18	-
υ_{42}	β(N-O)(10)	851	854	872	856	1.00	6.52
υ_{43}	τ(ring) (25)	827	-	849	837	12.87	-
υ_{44}	β(C-N)$_{\text{in plane}}$(36)	776	776	796	777	21.86	11.38
υ_{45}	β(C-O)$_{\text{in plane}}$(42)	763	-	785	766	48.97	-
υ_{46}	β(N-O) (28)	749	753	766	745	75.94	35.45
υ_{47}	υ(C-H)(18)	718	-	740	721	5.81	-
υ_{48}	β(C-C-C)(23)	706	706	722	707	0.42	364.48
υ_{49}	β(C-C-C)(34) + υ (C-C)(21) + β (C-N)(10)	689	692	713	696	11.10	579.50
υ_{50}	γ(NH)(27)	629	630	651	638	14.05	55.86
υ_{51}	β(O-C-C)(62)+ β (C-C-H)(49)	618	616	640	625	0.33	32.86
υ_{52}	β(NH_2)(35) + β(C-O)(21)	596	-	613	599	5.19	-
υ_{53}	τ(NH_2)(36)	532	533	550	538	7.03	4.90
υ_{54}	β(C-C-C)(10)	508	506	523	511	0.15	4.49
υ_{55}	β(C-C-N)(18)	503	-	517	505	1.34	-
υ_{56}	υ(Pd-N)(33)	454	471	469	458	3.31	65.44
υ_{57}	τ(NH_2)(10)	441	444	457	448	57.33	67.02
υ_{58}	β(C-N)(34)	430	-	443	432	8.31	-
υ_{59}	β(C-N-N)$_{\text{in plane}}$(27)	422	-	436	426	0.47	-
υ_{60}	β(C-O)$_{\text{out of plane}}$(31)	415	-	425	417	9.98	-

3.2.5. CN vibrations

In the literature, there are numerous studies about CN stretching and bending modes. CN stretching modes appear in the region 1750–1600 cm^{-1} [55–57]. However, CN vibrations can be contamined with CC and CO vibrational modes since these vibrations are also observed in the same region as CN vibrational modes. Therefore, the identification of C-N stretching frequency is a very difficult task due to the mixing of bands. In this study, CN stretching mode was observed at 1632 cm^{-1} in the IR spectrum. The band was computed as 1632 cm^{-1}. The bending mode of the CN group was seen at 430 cm^{-1} in the IR spectrum and the band was calculated as 432 cm^{-1}. However, this bending mode was not observed in the Raman spectrum. The frequencies 776 cm^{-1} observed in the both IR spectrum and Raman spectrum could be assigned to the out-of-plane bending mode of CN.

3.2.6. CO vibrations

CO stretching mode of title compound was observed at 1676 cm^{-1} in the IR spectrum and observed at 1668 cm^{-1} in the Raman spectrum. The band was calculated as 1676 cm^{-1}. More-

over, CO in plane and out plane vibrations were seen at 763 and 415 cm^{-1}, respectively. However, these bands were not observed in the Raman spectrum.

3.2.7. CC vibrations

Aromatic CC stretching modes are observed between 1625 cm^{-1} and 1315 cm^{-1}in the infrared spectra [56]. In the literature, CC stretching wavenumbers were appeared in the range from 1650 to 900 cm^{-1} [58,59]. In this study, CC stretching vibrations have variable intensity and these vibrations were appeared between 1604 cm^{-1} and 997 cm^{-1} as seen in Table 3. The CC stretching modes showed pure modes, however certain of these vibrations are contaminated with other vibrations. These values are in agreement with literature [60,61].

The root-mean square deviation (RMSD) is evaluated and the correlation coefficient R is calculated for the compound. This RMSD value helps to understand the appreciable errors between theoretical and experimental wavenumbers [62].

$$RMSD = \sqrt{\frac{\sum_i^n \left(\nu^{cal} - \nu^{exp}\right)^2}{n}}$$

An error of 4.215 for FT-IR and 9.323 for Raman data is observed from RMSD value and the error may be because the experimental data is taken in solid phase whereas the computed data is in the gaseous phase. The correlation diagram of FTIR and FT-Raman is given in Fig. S3.

3.3. NMR studies of title compound

Proton (^{1}H) NMR spectrum of title molecule is given in Fig. S4. As seen in Fig. S4, The chemical shift of H57 and H41 atoms was found higher than other hydrogen atoms due to nitrogen and palladium atoms. H40 proton peak was observed at 10.71 ppm as a broad singlet peak. H57 and H41 atoms were appeared at 6.95 ppm as a broad singlet peak because of relaxation times. The chemical shifts values of aromatic protons are generally situated between 8.00 and 7.00 ppm. However, these chemical shift values can change depending on electronic environments of protons [63]. Signals of the protons H49, H50 (8.34 ppm) and H48, H51(8.07 ppm), deshielded to higher chemical shifts by the nitro and the carbonyl group, respectively, appear as doublets due to the vicinal coupling (H48, H49 and H50, H51). Chemical environments of H10&H11, H21&H22 and H32&H33 atoms are similar to each other and so proton peaks of these atoms are overlapped. Moreover, these atoms were observed at 7.65 ppm as triplet because of other hydrogen atoms of aromatic ring. A similar situation was observed for H6&H8, H17&H19 and H28&H30. These atoms also were appeared at 7.49 ppm as doublet. H12, H23 and H34 atoms were seen at 7.54 ppm (Fig. S4).

Carbon (^{13}C) NMR spectrum of title molecule is given in Fig. S5. As seen in Fig. S5, the chemical shift of C52 atom was found higher than other carbon atoms due to nitrogen and oxygen atoms. The one was observed at 163.13 ppm. C44 atom was appeared at 149.21 ppm. Since it is attached to the nitro group, it has shifted to the low magnetic field region. C47 atom was seen at 138.87 ppm. C2, C13 and C24 atoms bonded to phosphorus atom are similar to each other as chemical environment and so peaks belong to these atoms were observed as overlapped and observed at 134.50 ppm. Chemical shift values the carbon atoms in the title compound are given in Table 4.

COSY (Correlation Spectroscopy) NMR experiment is good for determining basic connectivity via J-couplings (through bond) [64]. All the connections between hydrogen atoms in the title compound were clearly observed in the COSY (^{1}H-^{1}H) NMR spectrum (Fig. 7). As seen in COSY NMR spectrum of title compound, The neighborhoods between hydrogen atoms are observed as follows: H49, H50→H48, H51 and H12, H23, H34→ H32&H33, H21&H22, H10&H11.

HMBC NMR experiment detects heteronuclear correlations over-longer ranges of about 2-4 bonds [65]. HMBC NMR spectrum of title compound is given in Fig. 7. As seen in HMBC (^{1}H-^{13}C) NMR spectrum (Fig. 7), C45 and C43 atoms neighbor to H49 and H50 atoms from 1 bond distance and so C45, C43→H49, H50 connection can clearly be seen. Moreover, C42, C46→H48, H51 and C31, C20, C5→H10, H23, H34 connections also can be observed in the HMBC spectrum.

^{1}H and ^{13}C chemical shift values of title compound were computed by B3LYP/6-311++G(d,p) level of theory in DMSO solvent environment (Table S1). In order to calculate the isotropic chemical shifts related to TMS, the isotropic shielding values were used [66].

$$\delta_{ISO}^{X} = \sigma_{ISO}^{TMS} - \sigma_{ISO}^{X}$$

In order to determine the correlation between experimental and theoretical chemical shift values of title compound, correlation graphs were prepared and given in Fig. S6.

Table 4
Calculated energy values of complex using B3LYP/LanL2DZ method

Calculated Energies	Values
E_{HOMO} (eV)	-7.92
E_{LUMO} (eV)	-2.70
Ionization potential (I) (eV)	7.92
Electron affinity (A) (eV)	2.70
Energy gap (ΔE) (eV)	5.22
Electronegativity (χ) (eV)	5.31
Chemical potential (μ) (eV)	-5.31
Chemical hardness (η) (eV)	2.61
Chemical softness (s) (eV)	0.19
Electrophilicity index (w) (eV)	5.41
Max. charge transfer (ΔN_{max})	1.02

Table S1
Experimental and theoretical NMR chemical shifts of title compound

Atoms	Chemical Shifts (ppm)	
	Experimental	B3LYP/6-311++G(d,p)
H40	10.71	12.64
H49, H50	8.34	9.12
H48, H51	8.07	9.10
H10, H11	7.65	8.04
H21, H22	7.65	8.04
H32, H33	7.65	8.04
H12, H23, H34	7.54	7.96
H6, H8	7.49	7.88
H17, H19	7.49	7.88
H28, H30	7.49	7.88
H57, H41	6.95	8.01
C52	163.13	172.28
C44	149.21	155.23
C47	138.87	147.96
C2, C13, C24	134.50	138.41
C5, C7	131,16	136.60
C16, C18	131,16	136.60
C27, C29	131,16	136.60
C42, C46	129.32	134.28
C3, C4	127.89	131.14
C14, C15	127.89	131.14
C25, C26	127.89	131.14
C43, C45	121.24	126.07

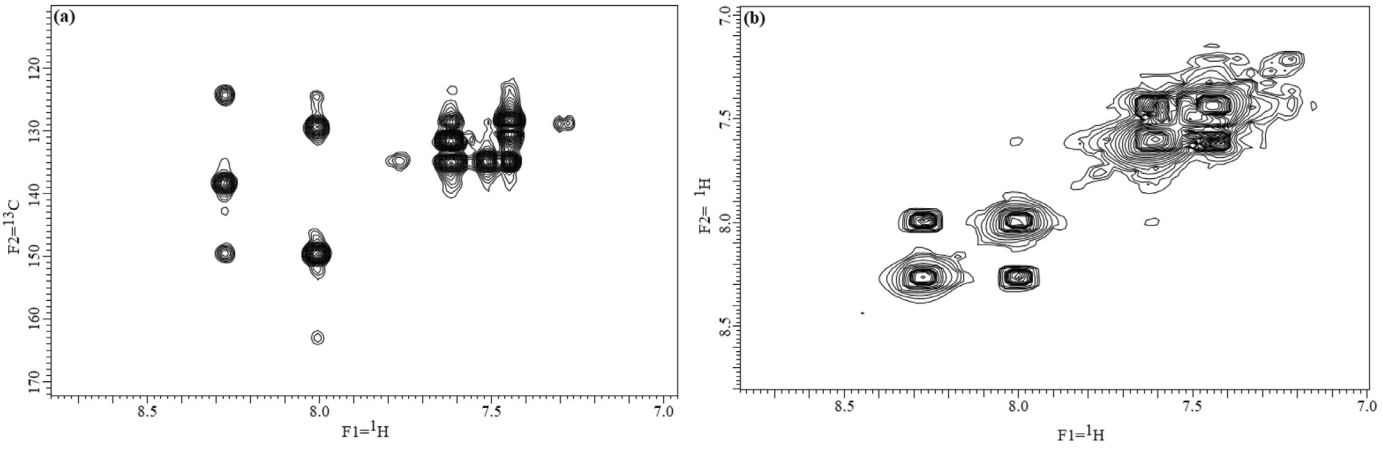

Fig. 7. HMBC (a) and COSY (b) NMR spectra of title compound in DMSO.

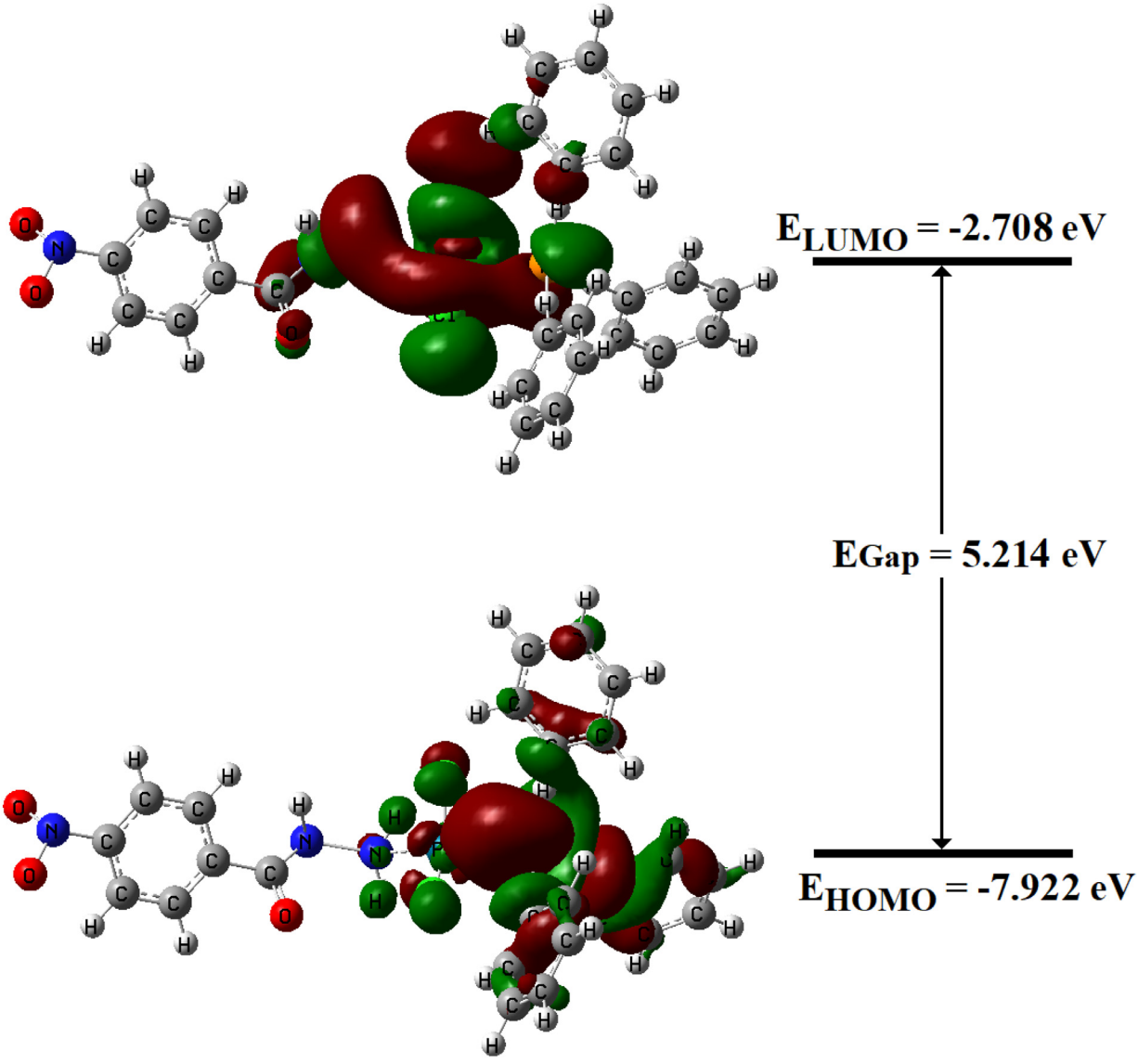

Fig. 8. HOMO and LUMO nodes and energy gap of title compound.

3.4. HOMO-LUMO energy gap

LUMO, HOMO energy values and energy gap give important information about optical properties, chemical stability and molecular electrical transport properties of molecules [67,68]. The energy values of the highest occupied molecular orbital (HOMO) and the lowest unoccupied molecular orbital (LUMO) of title compound were computed by B3LYP/LanL2DZ level of theory. The relevant molecular orbital plots of the HOMO and LUMO for title compound are given in Fig. 8. HOMO and LUMO energies values of the title molecule were calculated as -7.922 eV and -2.708 eV, respectively. The energy gap between HOMO and LUMO was computed as 5.214 eV. Nodes of HOMO were located on the Pd and P atoms and also carbon atoms of rings, whereas nodes of LUMO were located on the oxygen, palladium and phosphorus atoms.

3.5. Thermal analysis

Thermal behavior of the complex was investigated by TG and DTG methods in the temperature range from 25 to 600 °C in a nitrogen atmosphere. Thermal decomposition curve of the complex is given in Fig. S7. The complex is stable up to 205 °C and then begin to decompose. Endothermic decomposition of H_2O [Found (Calc.)(%): 2.55 (2.13)] was observed. Endothermic decompositions of ligand molecules [Found (Calc.)(%): 21.18 (24.34)] and [Found (Calc.)(%): 41.45 (43.66)] were seen in the temperature range from 205 to 252 °C and range from 252 to 375 °C, respectively.

3.6. Global chemical activity

The chemical reactivity of a molecule is determined by the energy gap of that molecule between HOMO and LUMO and chemical reactivity is determined by chemical potential (μ) and electrophilicity index (w). The w value is related to the tendency of electrons in the molecule to escape from the molecule. Moreover, chemical reactivity can explain global chemical hardness (η), chemical potential (μ) and global electrophilicity index (W). Global chemical hardness allows the determination of the resistance to the redistribution of electrons in the molecule. Moreover, ionization potential (I) is expressed as $I = -E_{HOMO}$ and electron affinity (A) is expressed as $A = -E_{LUMO}$. Such values are calculated as follows [69,70];

$$X = \frac{(I+A)}{2}$$

$$\mu = -\frac{(I+A)}{2}$$

$$\eta = \frac{(I-A)}{2}$$

$$S = \frac{1}{2\eta}$$

$$W = \frac{\mu^2}{2\eta}$$

$$\Delta N_{max} = \frac{(I+A)}{2(I-A)}$$

In this study, title molecule has higher chemical reactivity and lower kinetic stability because of the fact that energy gap value of title molecule is high value. All of the values are shown in Table 4.

Density of states (DOS) show number of states in unit energy interval. DOS can give information about state distribution of molecular systems. Moreover, it is important for optical transition probabilities. In this study, DOS analysis of complex was calculated at B3LYP/LanL2DZ level of theory in the gas phase. DOS analysis curve of title compound is given in Fig. S8. This analysis shows that maximum density of states lies over occupied orbitals with energy range of -20 eV and 0 eV.

4. Conclusion

In this study, A new Pd(II)-Hydrazide-Triphenylphosphine complex was synthesized and characterized by various spectroscopic techniques including single crystal XRD, FT-IR, Raman and NMR. Some geometric parameters and vibrational wavenumbers of title molecule were computed with the DFT-B3LYP method using 6-311G++(d,p) and the LANL2DZ basis set. Obtained experimental results were compared with theoretical results and it was concluded that theoretically obtained results have a good confirmation with experimentally obtained results. Energy gap was calculated as 5.218 eV. It was clear that title molecule has higher chemical reactivity and lower kinetic stability because of the fact that energy gap value of title molecule is high value. The X-ray structure is slightly different from its optimized molecular structures because the crystal structure in the solid phase is stabilized by the intermolecular C-O…H, N-O…H and N-O…H hydrogen bonds that supply the leading contribution to stability.

Declaration of Competing Interest

The authors declare that they have no known competing financial interests or personal relationships that could have appeared to influence the work reported in this paper.

CRediT authorship contribution statement

Gökhan Dikmen: Supervision, Investigation, Software, Methodology, Formal analysis, Writing - original draft. **Hakan Ünver:** Formal analysis, Investigation, Methodology, Writing - original draft.

Acknowledgements

The authors thankfully acknowledge the Medicinal Plants and Medicine Research Centre of Anadolu University, Eskişehir, Turkey for the use of X-ray Diffractometer and Eskişehir Osmangazi University, Central Research Laboratory Application and Research Center (ARUM) Eskişehir, Turkey for the other spectroscopic measurements. This study was supported by the Scientific Research Projects Commission of Eskisehir Technical University as a Project no 19ADP061.

Supplementary materials

Supplementary material associated with this article can be found, in the online version, at doi:10.1016/j.molstruc.2020.129139.

References

[1] M. Bakir, M.W. Lawrence, P. Nelson, M.B. Yamin, Catalytic C-C cross-coupling and hydrogen evolution by two Pd(II)-complexes of di-2-pyridyl ketone benzoyl hydrazones, J. Coord. Chem. 72 (2019) 2261–2278.
[2] H. Kargar, V. Torabi, A. Akbari, R. Behjatmanesh-Ardakani, A. Sahraei, M.N. Tahir, Synthesis, crystal structure, spectroscopic investigations, and computational studies of Ni(II) and Pd(II) complexes with asymmetric tetradentate NOON Schiff base ligand, Struct. Chem. 30 (2019) 2289–2299.
[3] H. Kargar, V. Torabi, A. Akbari, R. Behjatmanesh-Ardakani, M.N. Tahir, Synthesis, characterization, crystal structure and DFT studies of a palladium(II) complex with an asymmetric Schiff base ligand, J. Mol. Struct. 1179 (2019) 732–738.
[4] G. Dikmen, D. Hür, Palladium(II) complex: Synthesis, spectroscopic studies and DFT calculations, Chem. Phys. Lett. 716 (2019) 49–60.
[5] A. Kumar, A. Naaz, A.P. Prakasham, M.K. Gangwar, R.J. Butcher, D. Panda, P. Ghosh, Potent anticancer activity with high selectivity of a chiral palladium N-heterocyclic carbene complex, ACS Omega 2 (8) (2017) 4632–4646.

[6] E. Gao, Y. Sun, Q. Liu, L. Duan, An anticancer metallobenzylmalonate: crystal structure and anticancer activity of a palladium complex of 2,2′-bipyridine and benzylmalonate, J. Coord. Chem. 59 (11) (2006) 1295–1300.

[7] Z. Muhi-Eldeen, K. Al-Obidi, M. Nadir, F. Rochev, Synthesis and antimicrobial activity of Ni(II), Co(II), Zn(II) and Cd(II) complexes of 4-substituted-3-mercapto-5-phenyl-4H-1,2,4-triazoles, Eur. J. Med. Chem. 27 (1992) 101–106.

[8] J. Martinez, A. Martinez, M.L. Cuenca, A.D. Lopez, Synthesis, thermal and spectral study of oxovanadium (IV) complexes with benzoic acid hydrazine and p-hydroxybenzoic acid hydrazide, Synth. React. Inorg. Met.-Org. Chem. 18 (1988) 881–901.

[9] C.G. Hızlıateş, Arylidene carbazole carbohydrazides: synthesis and characterization, Hacettepe J. Biol. & Chem 46 (2) (2018) 169–175.

[10] M.S. Khan, S.P. Siddiqui, N. Tarannum, A systematic review on the synthesis and biological activity of hydrazide derivatives, Hygeia. J. D. Med. 9 (1) (2017) 61–79.

[11] L.M. Sousa, A.L.B.Formiga P.P.Corbi, I.M.Marzano MarceloLancellotti, G.Von Poelhsitz E.C.Pereira-Maia, W. Guerra, Spectroscopic characterization and molecular modeling of novel palladium(II) complexes with carbazates and hydrazides, J. Mol. Struct. 1097 (2015) 15–22.

[12] E.H.S. Sousa, F.G.M. Vieira, J.S. Butler, L.A. Basso, D.S. Santiago, I.C.N. Diógenes, L.G.F. Lopes, P.J. Sadler, [Fe(CN)5(isoniazid)]3−: an iron isoniazid complex with redox behavior implicated in tuberculosis therapy, J. Inorg. Biochem. 140 (2014) 236–244.

[13] E.H.S. Sousa, L.A. Basso, D.S. Santos, I.C.N. Diógenes, E. Longhinotti, L.G.F. Lopes, I.S. Moreira, Isoniazid metal complex reactivity and insights for a novel anti–tuberculosis drug design, J. Biol. Inorg. Chem. 17 (2012) 275–283.

[14] Q.U. Ain, U. Ashiq, R.A. Jamal, M. Saleem, M.M. Tahir, Alpha-glucosidase and carbonic anhydrase inhibition studies of Pd(II)-hydrazide complexes, Arab. J. Chem 10 (4) (2017) 488–499.

[15] C.M. Manzano, F.R.G. Bergamini, W.R. Lustri, A.L.T.G. Ruiz, E.C.S.D. Oliveira, M.A. Ribeiro, A.L.B. Formiga, P.P. Corbi, Pt (II) and Pd(II) complexes with ibuprofen hydrazide: characterization, theoretical calculations, antibacterial and antitumor assays and studies of interaction with CT-DNA, J. Mol. Struct. 1154 (2018) 469–479.

[16] N. Dodoff, K. Grancharov, N. Spassovska, Platinum(II) complexes of 4-methoxy- and 4-chlorobenzoic acid hydrazides. Synthesis, characterization, and cytotoxic effect, J. Inorg. Biochem. 60 (1995) 257–266.

[17] K.K. Narang, V.P. Singh, Synthesis, characterization, thermal studies and biological activity of Iron (III) complexes with some acylhydrazines, Synth. React. Inorg. Met.-Org. Chem 23 (1993) 971–989.

[18] P. Sur, S.P. Chatterjee, P. Roy, B. Sur, 5-Nitrofuran derivatives of fatty acid hydrazides induce differentiation in human myeloid leukaemic cell lines, Cancer Lett. 94 (1995) 27–32.

[19] G.D. de Souza, M.A. Rodrigues, L.E. Fernandes, P.P. Silva, R. Ruggiero, E.C. Pereira-Maia, W. Guerra, Complexes of platinum and palladium with 4-nitrobenzoic hydrazide:synthesis and cytotoxic activity, Cent. Eur. J. Chem. 11 (2) (2013) 290–294.

[20] P. Drozdzewski, H. Maniak, M. Kubiak, The X-ray revision of the structure of bis(4-hydroxybenzhydrazide)copper(II) sulfate(VI) dihydrate and its vibrational spectroscopy, Struct. Chem. 21 (2) (2009) 405–414.

[21] H. Zaslona, P. Drozdzewski, K. Slepokura, The X-ray structures, vibrational spectroscopy and antimicrobial activity of nickel(II) complexes with 4-hydroxybenzhydrazide, J. Mol. Struct. 1100 (2015) 34–42.

[22] W.Z. Lee, H.S. Tseng, M.Y. Ku, T.S. Kuo, Dinickel complexes of disubstituted benzoate polydentate ligands: mimics for the active site of urease, Dalton Trans. 19 (2008) 2538–2541.

[23] Ö. Alver, G. Dikmen, FT-IR NMR, Raman and UV–Vis spectroscopic investigation and DFT study of 6-Bromo-3-Pyridinyl boronic acid, J. Mol. Struct. 1099 (2015) 625–632.

[24] Ö. Alver, G. Dikmen, Structure analysis and spectroscopic characterization of 2-Fluoro-3-Methylpyridine-5-Boronic Acid with experimental (FT-IR, Raman, NMR and XRD) techniques and quantum chemical calculations, J. Mol. Struct. 1108 (2016) 103–111.

[25] G. Dikmen, Experimental nuclear magnetic resonance spectral assignments, $^{1}H/^{13}C$ GIAO calculations, molecular structure and molecular resonance states of 4-Methyl-1H-Indazole-5-Boronic acid, J. Mol. Struct. 1156 (2018) 136–145.

[26] Y.M. Rong, S. Yu, X.Y. Jin, Vibrational spectroscopic, NMR parameters and electronic properties of three 3-phenylthiophene derivatives via density functional theory, SpringerPlus 3 (2014) 701–713.

[27] Y. Yang, H. Gao, Comparison of DFT methods for molecular structure and vibration spectra of ofloxacin calculations, Spectrochim. Acta A 85 (2012) 303–309.

[28] G. Dikmen, 4-Methyl-1H-Indazole-5-Boronic acid: Crystal structure, vibrational spectra and DFT simulations, J. Mol. Struct. 1150 (2017) 299–306.

[29] V.S. Sharma, A.S. Sharma, R.H. Vekariya, Columnar self-assembly of bowl-shaped luminscent oxadiazole calix[4]arene derivatives, J. Mol. Liq. 271 (2018) 319–327.

[30] SMART, Bruker AXS, 2000.

[31] O.V. Dolomanov, L.J. Bourhis, R.J. Gildea, J.A.K. Howard, H. Puschmann, OLEX2: a complete structure solution, refinement ans analysis program, J. Appl. Cryst. 42 (2009) 339–341.

[32] G.M. Sheldrick, SHELXS-97, Program for Crystal Structure Solution, University of Gottingen, 1997.

[33] G.M. Sheldrick, Crystal structure refinement with SHELXL, Acta Crystallogr. C64 (2015) 3–8.

[34] Mercury, visualization and analysis of crystal structures, J. Appl. Cryst. 39 (2006) 453–457.

[35] M.J. Frisch, et al., Gaussian 09, Revision A. 1, Gaussian, Inc, Wallingford, CT, 2009.

[36] S.R. Whittleton, R.J. Boyd, T.B. Grindley, Evaluation of effective core potentials and basis sets for the prediction of the geometries of alkyltin halides, J. Phys. Chem. A 110 (2006) 5893–5896.

[37] G. Rauhut, P. Pulay, Transferable scaling factors for density functional derived vibrational force fields, J. Phys. Chem. 99 (10) (1995) 3093–3100.

[38] J. Baker, A.A. Jarzecki, P. Pulay, Direct scaling of primitive valence force constants: an alternative approach to scaled quantum mechanical force fields, J. Phys. Chem. A 102 (8) (1998) 1412–1424.

[39] P. Pulay, G. Fogarasi, G. Pongor, J.E. Boggs, A. Vargha, Combination of theoretical ab initio and experimental information to obtain reliable harmonic force constants. Scaled quantum mechanical (QM) force fields for glyoxal, acrolein, butadiene, formaldehyde, and ethylene, J. Am. Chem. Soc. 105 (1983) 7037–7047.

[40] P. Pulay, G. Fogarasi, Geometry optimization in redundant internal coordinates, J. Chem. Phys. 96 (1992) 2856–2860.

[41] H. Ünver, X-ray structure of palladium (II) complex and its catalytic activity on Suzuki–Miyaura reaction under mild conditions, Res. Chem. Intermediat 44 (2018) 7835–7846.

[42] Ö. Alver, FT-IR, Raman and DFT studies on the vibrational spectra of 2,2-Bis(Aminoethoxy)Propane, Bull. Chem. Soc. Ethiop. 30 (1) (2016) 147–151.

[43] K. Druzbicki, E. Mikuli, Experimental (FT-IR and FT-RS) and theoretical (DFT) studies of molecular structure and internal modes of $[Mn(NH_3)_6](NO_3)_2$, Spectrochim. Acta A 77 (2010) 402–410.

[44] Ö. Alver, C. Parlak, Vibrational spectroscopic investigation and conformational analysis of 1-pentylamine: a comparative density functional study, J. Theor. Comput. Chem. 9 (2010) 667–685.

[45] Ö. Alver, C. Parlak, M. Şenyel, Theoretical and experimental vibrational spectroscopic study of 3-piperidino-propylamine, J. Mol. Struct. 923 (2009) 120–126.

[46] W. Hu, S.W. Deng, J.Y. Huang, Y.M. Lu, X.Y. Le, Intercalative interaction ofasymmetric copper(II) complex with DNA:Experimental, molecular docking,molecular dynamics and TDDFT studies, J. Inorg. Biochem. 127 (2013) 90–98.

[47] Y.R. Sharma, Elementary Organic Spectroscopy Principles and Chemical Applications, S. Chand&Company Ltd., New Delhi, 1994.

[48] S. Ramalingama, P. Anbusrinivasan, S. Periandy, FT-IR and FT-Raman spectralinvestigation, computed IR intensity and Raman activity analysis and frequency estimation analysis on 4-chloro-2- bromoacetophenone using HF and DFT calculations, Spectrochim. Acta A 78 (2011) 826–834.

[49] G. Socrates, Infrared and Raman Characteristic Group Frequencies Tables and Charts, third ed., Wiley, Chichester, 2001.

[50] G. Varsanyi, Vibrational Spectra of Benzene Derivatives, Academic Press, NewYork, 1969.

[51] Ö. Alver, G. Dikmen, Structure analysis and spectroscopic characterization of 2-Fluoro-3-Methylpyridine-5-Boronic Acid with experimental (FT-IR, Raman, NMR and XRD) techniques and quantum chemical calculations, J. Mol. Struct. 1108 (2016) 103–111.

[52] S. Sivaprakash, S. Prakash, S. Mohan, S.P. Jose, Quantum chemical studies and spectroscopic investigations on 2-amino-3-methyl-5-nitropyridine by density functional theory, Heliyon 5 (2019) e02149.

[53] C.V. Barra, O. Treu-Filho, F.V. Rocha, T.R. Moura, A.V.G. Netto, A.E. Mauro, J.C. Pinheiro, R.T. Kondo, Experimental and DFT study on the compounds $[PdCl_2L_2]$ (L = 4-methylpyrazole, 4-iodopyrazole), Acta Chim. Slov 62 (2015) 662–671.

[54] I. Gulaczyk, M. Kręglewski, A. Valentin, The N–N stretching band of hydrazine, J. Mol. Struct. 220 (1) (2003) 132–136.

[55] G. Socrates, Infrared and Raman characteristic group frequencies. 2004.

[56] R. Ramasamy, Vibrational spectroscopic studies of imidazole, Armen. J. Phys. 8 (1) (2015) 51–55.

[57] H. Günzler, H.U. Gremlich, IR Spectroscopy, John Wiley & Sons, 2002.

[58] J. Coates, Interpretation of Infrared Spectra, A Practical Approach, Encyclopedia of Analytical Chemistry: Applications, Theory and Instrumentation, John Wiley & Sons, 2006.

[59] E.C. Semidalas, C.E. Semidalas, Structure and vibrational spectra of p-coumaric acid dimers by DFT methods, Vib. Spectrosc 101 (2019) 100–108.

[60] V. Karunakaran, V. Balachandran, Experimental and computational study on molecular structure, natural bond orbital and natural hybrid orbital analysis of nonlinear optical material trans-3-(o-hydroxyphenyl-1-phenyl)-2-propen-1-one, J. Mol. Struct. 1053 (2013) 66–78.

[61] S. Ramalingam, S. Periandy, B. Elanchezhian, S. Mohan, FT-IR and FT-Raman spectra and vibrational investigation of 4-chloro-2-fluoro toluene using ab initio HF and DFT (B3LYP/B3PW91) calculations, Spectrochim. Acta Part A Mol. Biomol. Spectrosc 78 (2011) 429–436.

[62] V. Arjunan, P.S. Balamourougane, S. Thillai Govindaraja, S. Mohan, A comparative study on vibrational, conformational and electronic structureof 2-(hydroxymethyl)pyridine and 3-(hydroxymethyl)pyridine, J. Mol. Struct. 1018 (2012) 156–170.

[63] M. Senyel, Ö. Alver, C. Parlak, ^{1}H, ^{13}C, ^{15}N NMR and nJ(C, H) coupling constants investigation of 3-piperidino-propylamine: a combined experimental and theoretical study, Spectrochim. Acta A 71 (2008) 830–834.

[64] M. Ottiger, F. Delaglio, A. Bax, Measurement of J and dipolar couplings from simplified two-dimensional NMR spectra, J. Magn. Reson. 131 (2) (1998) 373–378.
[65] D.W.C. Tim, I. Pérez-Victoria, Enhanced ^{13}C resolution in semi-selective HMBC: a band-selective, constant-time HMBC for complex organic structure elucidation by NMR, Org. Biomol. Chem 21 (2003) 3632–3634.
[66] Y. Yesiltepe, J.R. Nunez, S.M. Colby, D.G. Thomas, M.I. Borkum, P.N. Reardon, N.M. Washton, T.O. Metz, J.G. Teeguarden, N. Govind, R.S. Renslow, An automated framework for NMR chemical shift calculations of small organic molecules, J. Cheminform 10 (52) (2018) 1–16.
[67] M. Prabhaharan, A.R. Prabakaran, S. Gunasekaran, S. Srinivasan, DFT studies on vibrational spectra, HOMO–LUMO, NBO and thermodynamic function analysis of cyanuric fluoride, Spectrochim. Acta A 136 (2015) 494–503.
[68] S. Gunasekaran, R.A. Balaji, S. Kumaresan, G. Anand, S. Srinivasan, Experimental and theoretical investigations of spectroscopic properties of N-acetyl-5-methoxytryptamine, Can. J. Anal. Sci. Spectrosc 53 (2008) 149–160.
[69] J. Bevan Ott, J. Boerio-Goates, Calculations from Statistical Thermodynamics, Academic Press, 2000.
[70] J.I. Ahamed, M. Priya, P. Vinothkumar, K. Sathyamoorthy, P. MuraliManohar, J. Liu, M.F. Valan, A combined experimental and DFT computations study of novel (E)-3-(benzofuran-2-yl)-2-(thiophen-2-yl)acrylonitrile(TACNBNF): Insight into the synthesis, single crystal XRD, NMR, vibrational spectral analysis, in vitro antioxidant and in silico molecular docking investigation with human peroxiredoxin 5 protein, J. Mol. Struct. 1202 (2020) 127241.